Crowding the Environment of Single-Chain Nano-Particles: A Combined Study by SANS and Simulations

Marina González-Burgos[1], Arantxa Arbe[1⋆], Angel J. Moreno[1], José A. Pomposo[1,2,3], Aurel Radulescu[4], and Juan Colmenero[1,3,5]

[1] *Centro de Física de Materiales (CFM) (CSIC–UPV/EHU) – Materials Physics Center (MPC), Paseo Manuel de Lardizabal 5, 20018 San Sebastián, Spain*

[2] *IKERBASQUE - Basque Foundation for Science, María Díaz de Haro 3, 48013 Bilbao, Spain*

[3] *Departamento de Física de Materiales (UPV/EHU), Apartado 1072, 20080 San Sebastián, Spain*

[4] *Jülich Centre for Neutron Science, Forschungszentrum Jülich GmbH, outstation at Heinz Maier-Leibnitz Zentrum, Lichtenbergstr.1, 85747 Garching, Germany*

[5] *Donostia International Physics Center, Paseo Manuel de Lardizabal 4, 20018 San Sebastián, Spain*

Abstract

We present an investigation, by combining small-angle neutron scattering (SANS) and coarse-grained molecular dynamics (MD) simulations, on the conformational properties of single-chain nano-particles (SCNPs) in crowded macromolecular solutions. By using linear chains as crowders SANS shows a crossover from almost unperturbed SCNP conformations in dilute conditions toward a continuous collapse of the macromolecule with increasing crowding. This collapse starts when the total concentration of the solution reaches the value of the overlap concentration of the pure SCNP solutions. MD-simulations suggest the generalizability of these experimental findings and extend them to the case when the SCNPs themselves are used as crowders –a situation which in real systems leads to unavoidable formation of aggregates, as shown here by SANS and DLS. Exploiting the simulations we have calculated the contact probability and the distance between monomers as functions of the contour distance between them; the results suggest that crumpled globular conformations are generally adopted by SCNPs in crowded macromolecular solutions. In the case of linear crowders, the SCNPs show, at fixed monomer concentration, a non-monotonic dependence of their collapse on the length of the crowders.

I. INTRODUCTION

Single Chain Nano-Particles (SCNPs) are polymeric soft nano-objects consisting of uni-macromolecular chains collapsed to a certain degree by means of intramolecular bonding (i.e., covalent, non-covalent or reversible covalent bonds). Sensing capabilities, controlled drug delivery and catalytic applications, among others, of single-chain nano-particles have been recently demonstrated in dilute conditions [1–10]. From a basic point of view, though some peculiarities of protein folding as e. g. small folding times and possibly two-state folding are obviously not reproduced, the folding/collapse process leading to nano-particle formation has attracted significant interest as a *simplified* model for such an important biological process. By combining small angle scattering experiments [both, by neutrons (SANS) and X-rays (SAXS)] with computer simulations and by analyzing a large number of systems reported in the literature, it has been shown that the usual techniques for SCNP formation in good solvent conditions result in sparse, non-globular morphologies in solution, even by employing highly-efficient intra-chain cross-linking techniques (e. g., 'click' chemistry) or supramolecular interactions [11]. The fundamental physical reason underlying this general observation is that the formation of long-range loops, leading to efficient folding into globular structures, is an infrequent event due to the self-avoiding conformations universally adopted by the linear precursors in good solvent conditions [12].

It is noteworthy that the global conformations exhibited by SCNPs in dilute solution share some structural features with those displayed by intrinsically disorder proteins (IDPs) [13]. IDPs are ubiquitous in nature and responsible of functions of utmost relevance in biological systems [14]. Their biological function is founded on their internal dynamics and flexibility, which enable them to respond quickly to environmental changes and to bind with different cellular targets. A first analogy between SCNPs and IDPs is the similar scaling behavior of their molecular size R with the number of monomers or residues N, $R \sim N^{\nu}$,with an average exponent $\nu \sim 0.5$ [11, 15, 16]. Another common feature with IDPs is that SCNPs are intrinsically polydisperse both in size and topology, even if they are produced by the same chemical route [11, 12, 17–19] (i.e., same chemistry, molecular weight and fraction of functional groups in the precursor). Though lacking of ordered structure, SCNPs still show weakly deformable domains (analogues of ordered IDP domains) [20]. We also note that dynamically, both SCNPs and IDPs seem to share a high degree of internal friction that

strongly hampers chain motions [21]. Despite the obvious existence of differences between synthetic SCNPs and IDPs –like e. g. the impossibility of unfolding irreversible SCNPs again, once the internal crosslink has been induced– the above described structural and dynamical similarities emphasizing the analogies between SCNPs and IDPs in dilute conditions can be invoked to consider SCNPs as model systems, free of specific interactions, to mimic properties of IDPs in different environments (crowding, confinement, etc).

Though the conformational, dynamic and catalytic properties of SCNPs at high dilution have been actively investigated over recent years, their eventual modification in concentrated solutions is a scarcely explored problem. Still, there are indications from other fields of research –in particular from the problem of crowding in cellular environments– that suggest that the former properties of SCNPs in concentrated solutions can significantly differ from those at high dilution. In crowded cellular environments highly concentrated macromolecular solutions, typically in the range of 100-400 mg/mL, are usually present. In such systems, macromolecular species as proteins and RNA occupy a large volume fraction (10 - 40%) of the cell [22, 23] and the typical size of a 'tagged' macromolecule is comparable to the typical distance between the crowders. The effective nano-confinement effect induced by the crowders can dramatically modify biological function, through changes in the conformational and dynamical properties of the macromolecules respect to diluted in vitro conditions (<10 mg/mL) [22–26]. Folding, structural stability and self-assembly of proteins can also be strongly affected by crowding [27–32]. Crowding effects can be particularly strong for the properties of IDPs [33–35], due to their aforementioned malleability and propensity to bind with different targets [29, 36].

One limiting case of increasingly crowding environment for SCNPs is when they are part of so-called all-polymer nano-composites i.e., linear polymeric matrices embedding SCNPs instead of the usual hard inorganic nano-particles. Actually, an important envisaged application of SCNPs from the earlier times was as components of such materials. This is due to several advantages presented by SCNPs; among them, we can highlight the following three: (i) their small size (tuneable by the molecular weight of the starting precursor chains), (ii) the possibility of removing incompatibility effects between the nano-composite components by choosing pairs of polymers with null or even negative values of the interaction parameter χ and (iii) the versatility of the final nano-composites concerning the relative hard/soft character of the components imprinted by tuning their glass transition temperatures. Up

to date, experimental information about the structural features and molecular dynamics in bulk materials containing SCNP (all-polymer nano-composites and bulk polymers composed by only SCNPs) is certainly scarce. However, intriguing results have been reported for all-polymer nano-composites. In the earliest work by Mackay and coworkers on systems based on polystyrene, an unexpected decrease in the viscosity was found [37]. More recently, a striking increase of the volume explored by the matrix linear polymeric chains [consisting of long poly(ethylene) (PEO) macromolecules] was directly observed by quasielastic neutron scattering techniques upon inclusion of SCNPs based on poly(methyl methacrylate) (PMMA) [38].

Inspired by the former analogies with IDPs and motivated by the previous intriguing findings on all-polymer nano-composites, we aimed to investigate the conformational properties of SCNPs in concentrated solutions as model systems of crowded environments. In a recent work [20], we presented a global picture for the conformational properties of SCNPs in solution, covering the whole concentration range from infinite dilution to bulk density. That study was mainly based on MD-simulations on solutions of SCNPs using a generic simple coarse-grained model ('bead-spring'). It was found that the SCNPs start to collapse above their overlap concentration $c^\star$ ($c^\star = M_w/[(2\overline{R}_g)^3 N_A]$ with M_w the molecular weight, $\overline{R}_g = \langle R_g^2 \rangle^{1/2}$ the average radius of gyration and N_A the Avogadro's number). Experimental small angle neutron scattering (SANS) results were also included in that work. The large difference in the average scattering length values of H and D ($\overline{b}_D$=6.67 fm vs $\overline{b}_H$=-3.74 fm) provides a unique tool for investigating soft materials by neutron scattering: deuterium labeling. It results in a marked difference in scattering power (contrast) between molecules synthesized from normal (protonated) and deuterated units. Thus, deuterium labeling techniques can be exploited to 'stain' molecules and make them 'visible' not only in dilute solutions, but also in crowded environments, such as concentrated solutions of overlapping chains and even in the condensed state. The SANS study presented in Ref. [20] corresponded only to two limit cases: high dilution of SCNPs in a good molecular solvent and a nano-composite formed by a PEO matrix and PMMA-based SCNPs –actually, the system exhibiting noteworthy dynamical effects previously commented [38]–. Interestingly enough, the SANS experiments on the nano-composite as well as the bead-spring simulations on SCNPs in bulk conditions (both in a melt of only SCNPs and in a nano-composite model combining SCNPs and linear precursor chains) revealed an unexpected 'crumpled' globu-

lar [39] morphology of the SCNPs, similar to that presented by ring polymers in melts [40, 41] and chromatin loops in chromosomes [42].

In this work we exploit neutron scattering selectivity achieved by isotopic (deuterium) labeling and present a SANS investigation on the conformational properties of SCNPs in increasingly crowded environments. Crowding is induced by two means, namely by adding either linear polymeric chains or SCNPs. A systematic complementary study by Dynamic Light Scattering (DLS) has also been carried out to determine under which conditions aggregation of the SCNPs takes place and its reversibility. Moreover, in order to generalize the experimental results, we have also carried out molecular dynamics (MD) simulations using a generic simple 'bead-spring' coarse-grained model. This model captures the universal monomer excluded volume and chain connectivity interactions, and it is free of specific interactions and of intra- and inter-molecular reactions in the solutions. We have also exploited the capabilities offered by the simulations in order to calculate observables that are not accessible by the SANS technique –namely the contact probability and the distance between monomers as functions of the contour distance between them– that allow discerning between an equilibrium or a fractal globule as the underlying conformational organization of the SCNPs in crowded environments.

The article is organized as follows. In Sections II and III we give experimental and simulation details, respectively. Results are described and analyzed in Section IV. General consequences of the former analysis are discussed in Section V. Conclusions are given in Section VI.

II. EXPERIMENTAL

A. Samples

We investigated SCNPs obtained starting from linear precursors (Prec) consisting of random copolymers of methyl methacrylate (MMA) and (2-acetoacetoxy)ethyl methacrylate (AEMA), namely P($MMA_{0.71}$-co-$AEMA_{0.29}$). Three different molecular weights for precursors were investigated. The molecular weights and polydispersities determined by SEC are displayed in Table I. SCNPs were obtained through two different cross-linking mechanisms. One of them was Michael addition-mediated multidirectional self-assembly. This protocol

Sample	M_w (g/mol)	M_w/M_n	$\overline{R}_g$ (nm)	ν	$c^\star$ (mg/mL)
Hi-Prec	271800	1.423	13.5±0.16	0.59±0.012	23 (14[a])
Hi-MNP			9.78±1.09	0.49±0.013	60
Me-Prec	123520	1.114	9.97±0.64	0.59±0.008	26
Me-MNP			7.21±0.11	0.46±0.013	68
Lo-Prec	52100	1.185	5.91±0.19	0.59±0.019	52
Lo-MNP			4.81±0.05	0.47±0.014	97
Me-dPMMA	99134	1.093	10.20±0.36	0.59±0.01	19
Lo-dPMMA	9595	1.109	3.07±0.16	0.59±0.013	69

TABLE I: Chain characteristics and overlap concentrations of precursors and SCNPs obtained through Michael addition as determined by SANS on solutions in dDMF at 5mg/mL. The results on the linear PMMA crowders are also shown. [a] Value obtained imposing the $\overline{R}_g \propto N^{0.59}$ law shown in Fig. 2.

was conducted at room temperature in tetrahydrofuran (THF, Scharlab) at 1 mg/mL during 72 h, by following the procedure reported in Ref. [43]. We will refer to the such obtained SCNPs as 'MNPs'. Trimethylolpropane triacrylate (TMT, Sigma-Aldrich, technical grade) acted as intrachain cross-linking agent. The other route was intrachain Cu(II) complexation of AEMA units, exploiting the β-ketoester functional groups in the copolymer precursors. Reaction times were of 24 h, at a concentration of 1 mg/mL in THF. The SCNPs synthesized by this method (described in detail in Ref. [2]) will be called 'CuNPs' throughout the manuscript. CuNPs were only investigated by DLS.

The SANS experiments on dilute solutions were carried out with deuterated N-N-Dimethylformamide (dDMF, 99.5% atom, from Across Organics) as solvent. Crowded solutions were obtained by adding deuterated linear PMMA chains of two different molecular weights (Polymer Source, see Table I).

To apply isotopic labeling for studying by SANS the effects produced by increasing the concentration of SCNPs, deuterated SCNPs were necessary. They were synthesized starting from linear precursors ('dPrec') consisting of deuterated MMA monomers, but the unavailability of deuterated AEMA monomers prevented to obtain completely deuterated macromolecules. The synthesis protocol was the same as that applied for intra-chain crosslinking

Sample	Formula	$\rho_s \times 10^{10}(\mathrm{cm}^{-2})$
PMMA	$[C_5H_8O_2]_n$	1.0593
PAEMA	$[C_{10}H_{14}O_5]_n$	1.5316
dPMMA	$[C_5D_8O_2]_n$	6.9685
TMT	$C_{15}H_{20}O_6$	1.3355
Prec	$[C_{6.45}H_{9.74}O_{2.87}]_n$	1.2577
MNP	$[C_{7.9}H_{11.39}O_{3.45}]_n$	1.3258
dMNP	$[C_{7.9}D_{5.68}H_{5.71}O_{3.45}]_n$	4.0255
DMF	C_3H_7NO	0.6941
dDMF	C_3D_7NO	6.3645

TABLE II: Chemical formulae and scattering length densities of the substances involved in the SANS experiments.

of the Michael-SCNPs previously described. Only high-molecular weight macromolecules (similar molecular weight as that of the protonated counterparts Hi-Prec) were investigated. The resulting SCNPs will be denoted as 'dMNP'.

DLS experiments were carried out on solutions of both, MNPs and CuNPs in N-N-Dimethylformamide (DMF, 99.9%, from Sigma Aldrich).

B. Small Angle Neutron Scattering

SANS experiments were performed on the instrument KWS-2 at the Forschungs-Neutronenquelle Heinz Maier-Leibnitz in Garching. A Q-range between 0.003 and 0.35 $\mathrm{Å}^{-1}$ was covered, with $\lambda = 5.27$ Å and using three sample-detector distances (SSD): 1.15, 5.76 and 19.76 m. The solutions were filled in 2 mm thick Hellma Quarz cells. Experiments were carried out at room temperature. The azimuthally averaged scattered intensities were obtained as function of the wave-vector Q. The signal from the background was measured under the same conditions and subtracted from the measurements on the solutions with labelled macromolecules. The scattering length densities of the different macromolecules and solvents involved in the SANS experiments are listed in Table II.

C. Dynamic Light Scattering

Dynamic light scattering (DLS) probes the relaxation of concentration fluctuations on mesoscopic time and length scales. In a homodyne experiment, the measured intensity autocorrelation function is given by

$$\frac{\langle I(Q,0)I(Q,t)\rangle}{\langle I\rangle^2} = 1 + f_c\left[\frac{S(Q,t)}{S(Q,0)}\right]^2 \tag{1}$$

with f_c an experimental factor and $S(Q,t)$ the Fourier transform of the density correlation function of the scattering medium:

$$S(Q,t) = \frac{\int_V \left[\rho(0,0)\rho(\vec{r},t)\right] e^{i\vec{Q}\vec{r}} d^3\vec{r}}{\langle\rho\rangle}. \tag{2}$$

Here $\rho(\vec{r},t)$ is the local density at position $\vec{r}$ at time t in the sample. The scattering vector Q for light scattering is given by $Q = 4\pi n_d \sin\theta/\lambda_o$, with λ_o the wavelength in vacuum and n_d the refractive index. The experiments were performed on a Malvern Zetasizer Nano ZS apparatus. At the experimental conditions employed [2θ=173°, λ_o=633 nm, n_d(DMF)=1.431], the Q-value explored was 0.00284Å^{-1}.

III. SIMULATIONS

We used a simple bead-spring model [44] for the polymer precursors, which were constructed as linear chains of $N = 200$ monomers. A fraction $f = 0.4$ of the monomers in the precursor were selected as reactive ones. They were randomly distributed along the backbone with the constraint that consecutive reactive monomers were not allowed, preventing trivial cross-links. In order to mimic implicit good solvent conditions, the non-bonded interactions between the monomers were given by a purely repulsive Lennard-Jones (LJ) potential:

$$V_{\rm LJ}(r) = 4\epsilon[(\sigma/r)^{12} - (\sigma/r)^6 + 1/4], \tag{3}$$

which was cut-off at $r_{\rm c} = 2^{1/6}\sigma$. We set $\epsilon = \sigma = 1$ as units of energy and distance, respectively. Qualitatively, in the fully-flexible bead-spring model σ represents a distance of the order of the Kuhn length [44], i.e., $\sigma \sim 1$ nm [45]. The interactions between connected monomers were given by a FENE potential [44]:

$$V_{\rm FENE}(r) = -\epsilon K_{\rm F} R_0^2 \ln\left[1 - (r/R_0\sigma)^2\right], \tag{4}$$

with $K_{\rm F} = 15$ and $R_0 = 1.5$. The use of the LJ and FENE potentials prevents strong fluctuations of the bonds and guarantees chain uncrossability [44]. After equilibration of the precursors, the formation of the SCNPs through irreversible intramolecular cross-linking was activated. Two reactive monomers formed a bond when their mutual distance was smaller than $r_{\rm b} < 1.3\sigma$, and they remained bonded (through the FENE potential) for the rest of the simulation. The reactive monomers were monofunctional, i.e, a reactive monomer was not allowed to form a new bond if it was already bonded to another reactive monomer. The precursors were coupled to the same thermal bath but no intermolecular interactions were implemented in the cross-linking runs. Thus, the precursors were propagated independently and cross-linking was purely intramolecular by construction. This corresponds to the ideal limit of infinite dilution, which was approached in the experimental synthesis, performed at $1mg/mL$, for which the formation of aggregates was negligible [43]. Further details of the model and cross-linking procedure can be found in Ref. [44].

Cross-linking of the SCNPs was completed in all cases. A total of 200 SCNPs were generated and used for the simulations of the solutions, where the intermolecular interactions were switched on. They were inserted in a cubic simulation box with periodic boundary conditions, at a density far below the overlap concentration (see below) and preventing concatenation. The simulation box was very slowly compressed and equilibrated at the different simulated concentrations, where the acquisition runs were performed. Concentrations are defined as $c = N_{\rm mon}/L^3$, with $N_{\rm mon}$ the total number of monomers in the box and L the box size. The selected cocentrations covered the whole range from high dilution ($c = 0.002$) to $c = 0.85$, which qualitatively corresponds to bulk density [44].

We also performed simulations of solutions containing both SCNPs and linear chains. Namely, we selected a subset of 40 of the former SCNPs and used linear bead-spring chains as crowders. In this case the box size was fixed so that the concentration of SCNP monomers was always $c = 0.008$. In analogy to the experiments, this is much lower than the SCNP overlap concentration $c^\star = 0.062$ (see Table III). The number of linear chains was increased to cover a broad range of total monomer (SCNP+linear) concentrations, from high dilution to concentrated solutions. We used three types of linear crowders, of $N = 10$, 50 and 800 monomers per chain. In all cases the equilibration runs were long enough to allow SCNPs and crowders to diffuse a distance of at least their own size. In analogy to the experiments, the overlap concentration of each macromolecule of N monomers is defined as $c^\star = N/(2\overline{R}_g)^3$,

System	N	$\overline{R}_g$	$c^\star$
SCNP	200	7.4	0.062
LIN10	10	1.7	0.27
LIN50	50	4.8	0.057
LIN800	800	25.8	0.0058

TABLE III: Characteristics of the simulated SCNPs and linear chains: number of monomers N, average radius of gyration $\overline{R}_g$ and overlap concentration $c^\star$.

with $\overline{R}_g = \langle R_g^2 \rangle^{1/2}$ its average radius of gyration. For a correct comparison between the results in the pure solutions and in the mixtures, the static observables presented below for the pure solutions were averaged just over the set of 40 SCNPs that were also used in the mixtures. Still, very small differences were found by averaging over all the SCNPs in the pure solutions. Table III shows the average radii of gyration and overlap concentrations for the simulated SCNPs and linear crowders.

All the simulations (including the cross-linking runs) were performed under Langevin dynamics (see details in Ref. [12]) at temperature $T = 1$. A home-made code was used for the cross-linking simulations. The simulations of the solutions were performed by using the GROMACS 4.6.5 package [46]. Further simulation details can be found in Ref. [20].

IV. RESULTS

A. SANS on Michael-SCNPs in dilute conditions

A first set of SANS experiments was devoted to determine the size of the linear chains in dilute solution and the degree of collapse induced by the internal crosslinking procedure on the macromolecules. Since the scattered intensity is proportional to the square of the difference of the scattering length densities of the two phases A and B, $(\rho_s^A - \rho_s^B)^2$ (scattering contrast), these experiments were performed by dissolving protonated macromolecules in deuterated solvent. In this way, the contrast is highly enhanced (see Table II). As an example, for the macromolecules of highest molecular weight investigated, Fig. 1 shows the SANS results obtained before and after carrying out the crosslinking by Michael addition (samples Hi-Prec and Hi-MNP). The function measured for the precursor sample starts to

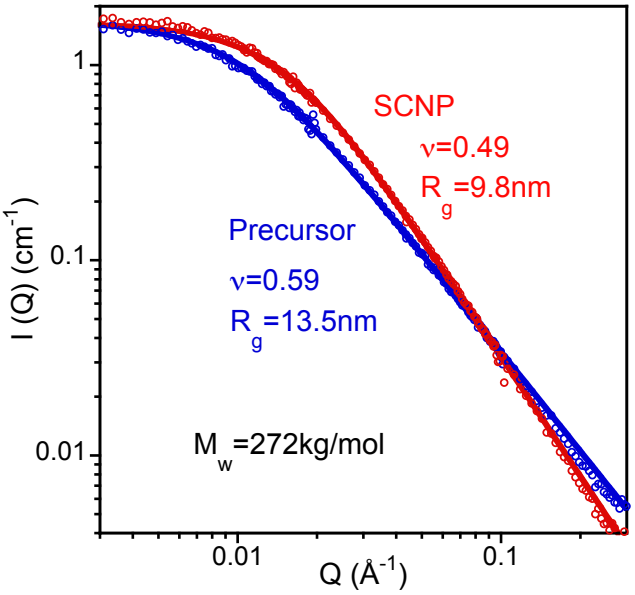

FIG. 1: Macromolecular form factors obtained by SANS on solutions (5mg/mL in dDMF) of linear precursor chains of M_w=272kg/mol and the corresponding SCNPs obtained by Michael addition. Lines are fits to generalized Gaussian form factors.

decay at lower Q-values than that obtained for the nanoparticles. We also see that the curves cross each other, due to an increase of the slope at intermediate Q-values upon crosslinking.

Under high dilution conditions of the labelled macromolecules, inter-molecular interactions are negligible and the associated structure factor is close to unity $S(Q) \approx 1$. Then, small angle scattering experiments provide full information about the size and shape of

these 'objects' since the scattered intensity $I(Q)$ directly reflects their form factor $P(Q)$ [$I(Q) \propto S(Q)P(Q) \approx P(Q)$]. Thus, the dimensions –quantified via the average radius of gyration $\overline{R}_g$– as well as the degree of compaction of the macromolecules– revealed by the scaling exponent ν that determines how the chain size depends on the number of monomers ($R \propto N^{\nu}$)– can easily be read out from the experimental results. On the one hand, the overall size determines the Q-range where the form factor decays. For bigger macromolecules, $P(Q)$ decays at smaller Q-values. On the other hand, the scaling exponent dictates the slope of this function at intermediate Q-values (there, $P(Q) \propto Q^{-1/\nu}$) [47]. Thus, from simple inspection of the results shown in Fig. 1 we can deduce that the chain dimensions are reduced and the macromolecule is more compact after the intra-molecular cross-linking procedure. In the two limiting cases of compaction for a macromolecule, namely the self-avoiding walk conformation adopted by a linear macromolecule in good solvent and the globular morphology, the scaling exponent takes the values of the Flory exponent ν_F=0.59 and ν_g=1/3 respectively. In the case of a *dense* spherical globule (with inner bulk density), an effective exponent $\nu = 0.25$ ($P(Q) \sim Q^{-4}$) is found due to surface Porod scattering, followed by harmonic oscillations at higher Q [47]. For the intermediate case of a random walk, representing the Gaussian conformation of a linear chain in a θ-solvent or in bulk, the scaling exponent is 1/2. In such a case, the form factor is described by the well-known Debye function:

$$P_{Debye}(Q) = \frac{2}{(\overline{R}_g^2 Q^2)^2}\left(e^{-\overline{R}_g^2 Q^2} - 1 + \overline{R}_g^2 Q^2\right) \tag{5}$$

The generalized Gaussian coil function [48]

$$P(Q) = \frac{1}{\nu U^{\frac{1}{2\nu}}}\gamma\left(\frac{1}{2\nu}, U\right) - \frac{1}{\nu U^{\frac{1}{\nu}}}\gamma\left(\frac{1}{\nu}, U\right) \tag{6}$$

where

$$U = \frac{(2\nu+1)(2\nu+2)}{6} Q^2 \overline{R}_g^2 \tag{7}$$

$$\gamma(a,x) = \int_0^x t^{a-1}\exp(-t)dt \tag{8}$$

allows for a description of the form factor for different values of the scaling exponent. It obviously reproduces the Debye function for ν=0.5. As can be seen in Fig. 1, this function describes well the experimental data and allows a precise determination of the values of $\overline{R}_g$ and ν. In the particular case shown in Fig. 1, $\overline{R}_g$ decreases from 13.5 nm to 9.8 nm and

the scaling exponent, which for the linear precursor chains adopts the expected value of ν_F=0.59, becomes 0.49 for the SCNPs.

Experiments in dilute conditions (5 mg/mL) were performed on precursors, SCNPs as well as on the linear deuterated PMMA chains that were used to induce crowding in the solutions (see Table I). In the later case, the solvent was protonated DMF to enhance the contrast for neutrons. The values obtained for $\overline{R}_g$ and ν are compiled in Table I. We also considered linear protonated PMMA chains of different molecular weights in deuterated DMF to increase the range of molecular weights explored. Figure 2 shows the macromolecular average size as a function of the main-chain length, represented by the number of main-chain bonds N. Within the uncertainties, we can see that the results on the linear macromolecules collapse on the top of the expected law $\overline{R}_g \propto N^{\nu_F}$. This implies that the length of the statistical segment for all these polymers is basically the same, independently of the presence of side groups. On the other hand, a certain collapse is achieved through the Michael addition method for the different macromolecular sizes investigated (see Table I and Fig. 2). However, the resulting morphology –characterized by ν = 0.46...0.49, see Table I– is still far from the globular one, as it is usually found [11]. As can be seen in Fig. 2, for the nano-particles the N-dependence of the size can be well described by $\overline{R}_g \propto N^{\nu=0.47}$, i. e., the macromolecular dimensions scale with an average value of the scaling exponents obtained for the three different molecular weights explored.

B. SANS on Michael-SCNPs in crowding conditions

1. Crowding with linear polymers

The effect of crowding the environment on the structure of SCNPs was first investigated by using linear polymeric chains (deuterated PMMA) as crowders. In a first set of SANS experiments, low-molecular weight chains (M_w ≈10 kg/mol) were added to dDMF-solutions of the three kinds of Michael SCNPs. The concentration of SCNPs, c_{SCNP}, was always kept fixed to c_{SCNP}=5 mg/mL of the total solution. This value is well below the overlap concentration of the SCNPs in the three cases [$c^{\star}_{SCNP}$=60, 68 and 97 mg/mL for Hi-MNP, Me-MNP and Lo-MNP respectively, see Table I]. The concentration of the crowder (c_{crow}) was varied between 0 and 395 mg/mL, such that the total polymer concentration c in the

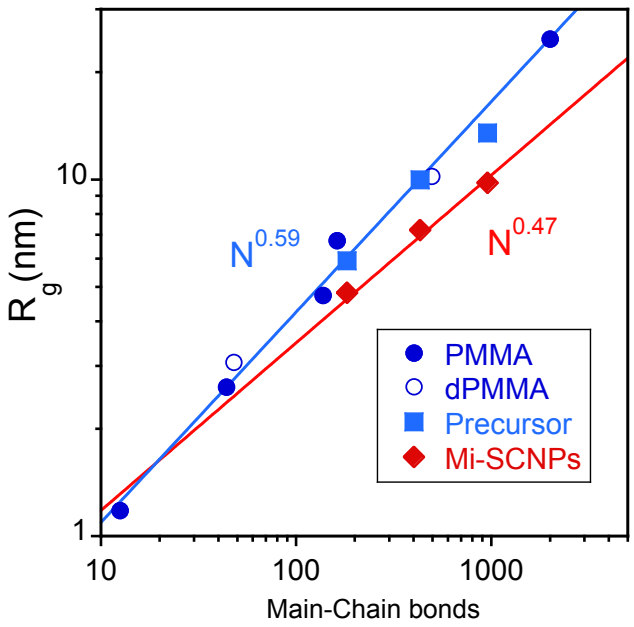

FIG. 2: Average radius of gyration obtained from the SANS experiments in high dilution as a function of the number of main-chain bonds for protonated PMMA (full circles), deuterated PMMA (empty circles), copolymer precursors (squares) and Michael SCNPs (diamonds). The protonated polymers were dissolved in deuterated DMF and the deuterated PMMA chains in protonated DMF. The lines are fits to power laws with fixed scaling exponents (0.59 for the linear chains and 0.47 for the SCNPs).

solution increased from 5 mg/mL up to 400 mg/mL. Given the low contrast between the crowders and the solvent (both deuterated), and the high contrast between the protonated SCNPs and the rest of the solution (Table II), the scattered intensity is overwhelmingly dominated by the contribution of the SCNPs against the surrounding medium. Moreover, as $c_{SCNP} << c^{\star}_{SCNP}$, inter-molecular correlations between SCNPs are expected to be negligible [$S(Q) \approx 1$] and thus the results directly reveal the SCNP form factor in the differently crowded solutions. For the intermediate molecular weight SCNPs investigated, Fig. 3 shows the SANS results for several concentrations. From the simple inspection of the curves, a decrease of the dimensions and of the scaling exponent of the SCNPs with increasing concentration can be directly deduced. The description of the results in terms of generalized Gaussian functions [Eqs. 6-8] delivered the values of $\overline{R}_g$ and ν represented in Fig. 4(b) as a function of the total polymer concentration in the solutions. As can be seen, above a given concentration range, both parameters decrease with increasingly crowded environment. The SCNP size reveals a clear shrink and the scaling exponent indicates an increasingly compaction upon crowding above such a concentration range. For high concentrations, values of ν close to the globular limit (ν_g=1/3) are reached. The experiments on the solutions with the same crowder and SCNPs of different sizes reveal a qualitatively similar behavior, as can be seen in Figs. 4(a) and (c).

Two concentrations might be invoked to be key ingredients in this situation: the overlap concentration of the SCNPs ($c^{\star}_{SCNP}$) and that of the crowders ($c^{\star}_{crow}$). From the $\overline{R}_g$-values obtained from the SANS experiments in dilute conditions, these values were calculated (see Table I). They are represented by the arrows in Fig. 4. They both are in the range where the crossover from unperturbed to collapsed dimensions take place, within the experimental uncertainties. Since for the chosen molecular weight of the crowder the differences between the values of its $c^{\star}$ and those of the SCNPs are not very large, it is not possible to univocally discern which one of the overlap concentrations plays the most important role in inducing the collapse of the SCNPs. It seems however that the crossover takes place in a concentration range that shifts toward larger values with decreasing molecular weight of the SCNPs, pointing to $c^{\star}_{SCNP}$ as the most plausible candidate for being the key magnitude.

To check this hypothesis we investigated the effects induced by much longer crowding chains –thereby with a much smaller overlap concentration $c^{\star}_{crow} << c^{\star}_{SCNP}$. This was realized for the case of the Me-MNPs, namely using dPMMA crowders with $M_w \approx$100 kg/mol.

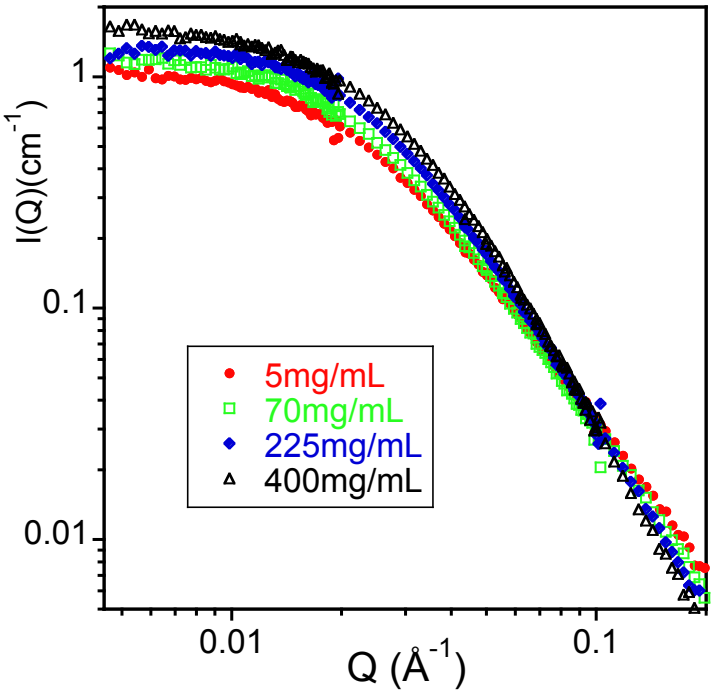

FIG. 3: Form factors of Michael SCNPs of M_w=124kg/mol (Me-MNPs) obtained by SANS on solutions in dDMF with increasing concentration (0, 65, 220 and 395 mg/mL) of low-molecular weight (M_w=10kg/mol) linear dPMMA; the SCNPs concentration is always 5 mg/mL (the legend indicates the *total* concentration of the solution).

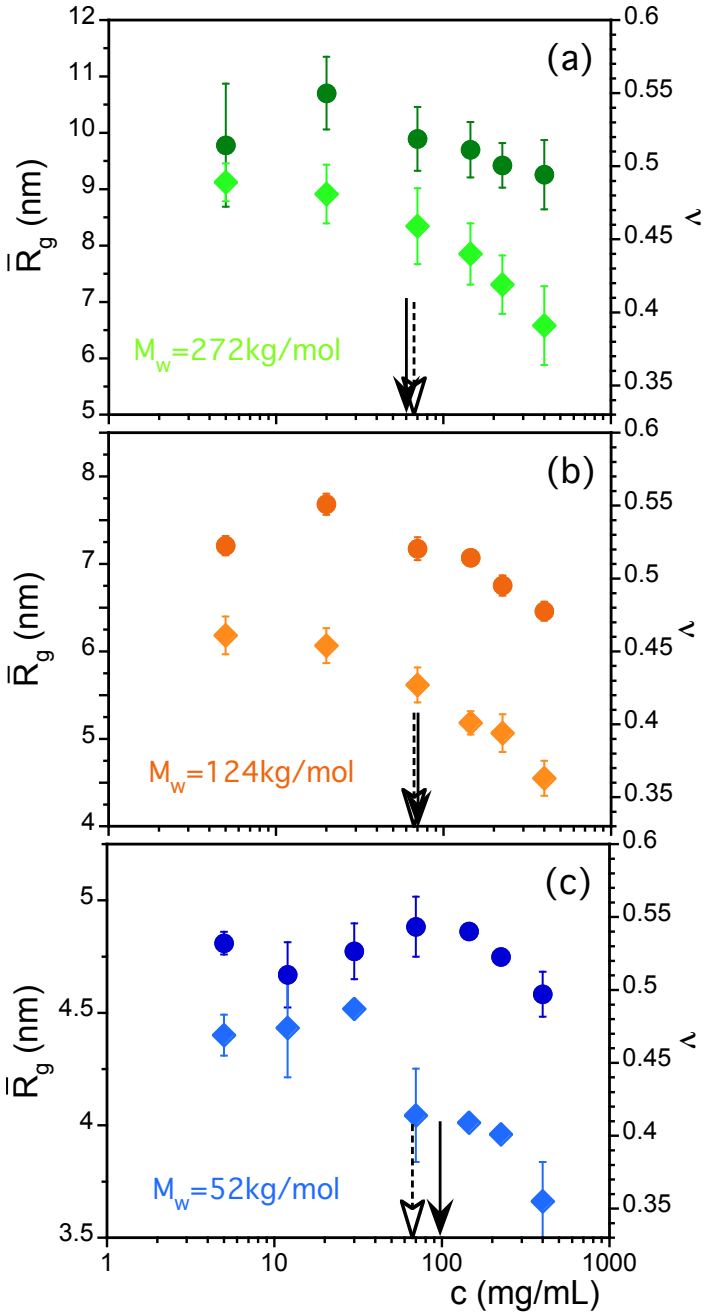

FIG. 4: Average radius of gyration (circles) and scaling exponent (diamonds) of the Michael SCNPs of M_w=272kg/mol (a), M_w=124kg/mol (b) and M_w=52kg/mol (c) as a function of the the total concentration. In all cases the crowders are the small dPMMA (M_w = 10 kg/mol). Vertical arrows show the location of the overlap concentration of the crowders (dashed) and of the SCNPs (solid).

As can be seen in Table I, for these chains $c^{\star}_{crow}$ = 19 mg/mL, more than three-fold lower than $c^{\star}_{SCNP}$. The determination of the SCNP size in these solutions was unfortunately subjected to large uncertainties due to an additional small-angle contribution which could be due to some remaining weak contrast between the big crowders and the solvent. Therefore, the analysis of the data was focused on the scaling exponent, which could still be determined with high accuracy. Figure 5 shows the concentration dependence of the scaling exponent ν of the SCNPs in the such crowded solutions. The compaction degree of the SCNPs is insensitive to the increase of the concentration across $c^{\star}_{crow}$. The crossover to collapsed conformations clearly starts at much higher concentrations, in a similar range than for the solutions with the low-molecular weight linear PMMA chains, coinciding, within the uncertainties, with $c^{\star}_{SCNP}$.

The construction of master plots for the size and scaling parameter (Fig. 6) against the reduced variable $c/c^{\star}_{SCNP}$ nicely supports this result. For constructing the master plot of the chain dimensions [Fig. 6(a)], we have normalized the average radii of gyration of the SCNPs to the values obtained for their dilute solutions without crowders (Table I). Since the value of ν at high dilution was very similar for the three molecular weights investigated, this variable was not renormalized in Fig. 6(b). The obtained master plots demonstrate that $c^{\star}_{SCNP}$ is the relevant magnitude determining the onset of collapse of the SCNPs.

2. Crowding with SCNPs

This was the situation investigated by MD-simulations in our earlier publication [20]. Similar experiments were intended with SCNPs as crowders. Realizing these experiments presented however several difficulties. When solutions with high concentrations of protonated macromolecules in deuterated solvent are investigated by SANS, the scattered intensity reveals not only the form factor of the individual nano-objects but also the structure factor, which cannot be approximated by unity anymore. To prevent this interference term, only few protonated macromolecules might be labelled in a deuterated sea –as in the situation investigated with dPMMA linear chains as crowders. However, since the functionalized AEMA groups and crosslinking agents could not be obtained in their deuterated forms, the 'deuterated' SCNPs (dMNPs) contained a non-negligible fraction of hydrogenated stuff. Therefore we performed the experiments dissolving a fixed amount of protonated MNPs (5 mg/mL)

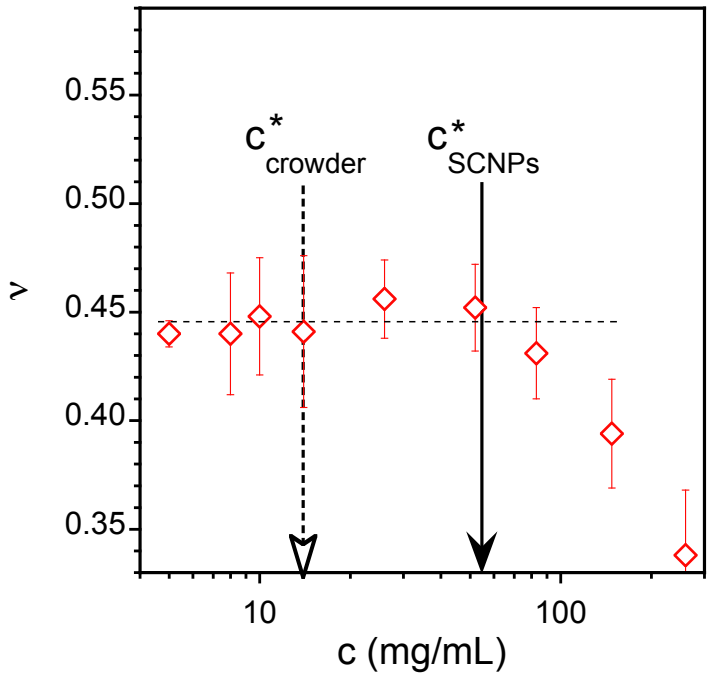

FIG. 5: Scaling exponent of the Michael SCNPs of M_w=124kg/mol in solutions with dPMMA of M_w=100 kg/mol as a function of the total concentration.

in solutions of dMNPs and mixtures of dDMF and DMF such that the dDMF/DMF ratio matched the dMNPs scattering. To find the matching conditions we first measured the scattering from solutions of dMNPs in different dDMF/DMF ratios. The coherently scattered intensity was minimal for a solution with a composition of 70%dDMF/30%DMF for the sol-

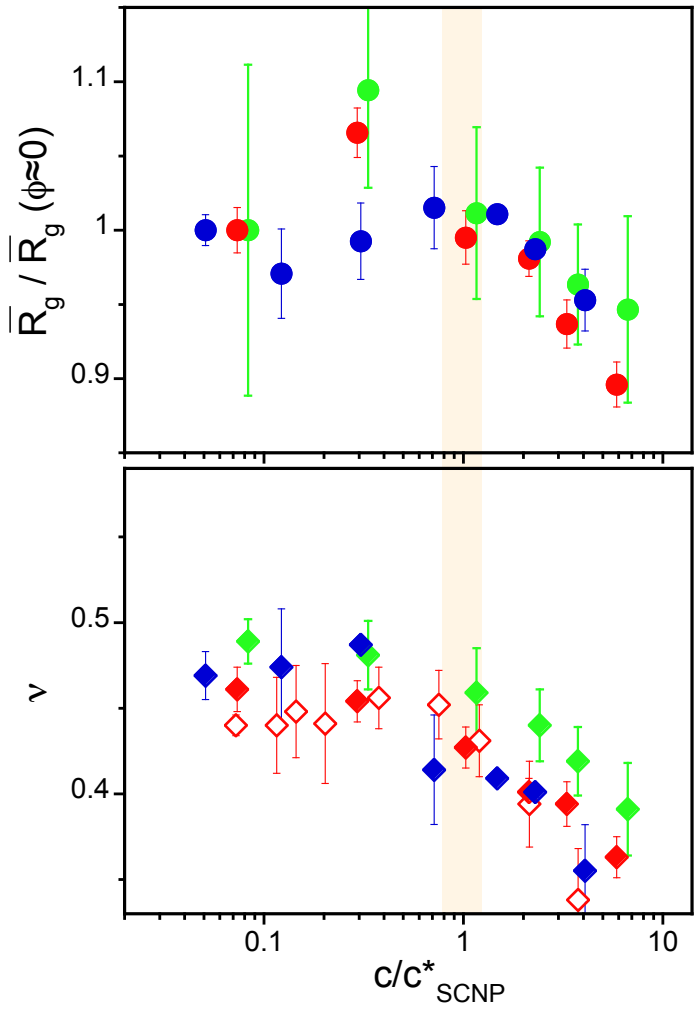

FIG. 6: Average radius of gyration normalized to its value at the lowest concentration investigated (a) and scaling exponent (b) of the Michael SCNPs as a function of the ratio between the total concentration and the overlap concentration of the SCNPs. Symbols as in Figs. 4 and 5.

vent. With this solvent ratio fixed, crowding was induced by increasing the concentration in dMNPs. The molecular weight considered in this kind of experiments was 272 kg/mol. After background corrections, the results are shown in Fig. 7(a) for some of the concentrations

investigated. They are supposed to be dominated by the contrast between the protonated SCNPs and the surrounding medium, revealing the form factor of the macromolecules. Superimposed to the expected result for the form factor, for all compositions there is a strong additional small-angle contribution, which prevents any reliable fit of the experimental data to Eqs. 6-8 and an accurate determination of the $\overline{R}_g$ and ν-values. The low-Q feature observed is indicative for the presence of extremely large objects in the solutions.

To discard the hypothesis that the small angle contribution could be an artifact of the kind of isotopic mixtures used, we also measured a solution of 35 mg/mL (about half the overlap concentration) of MNPs in dDMF. Figure 7(b) shows that the data obtained are also clearly affected by a strong increase of the intensity at small angles. Thus, there seems to be a strong tendency of SCNPs to aggregate in concentrated solutions.

From the slope of the curves in the fractal regime at intermediate Q-values we defined what we called an effective scaling exponent ν_{eff}. The inset in Fig. 7 displays the such obtained values. This parameter somehow should reflect the scaling exponent of the nanoparticles, but could be severely affected by (i) uncertainties in the subtraction of the high incoherent background; (ii) the low-Q contribution from the aggregates and, in the case of the measurements of the MNPs in dDMF at 35mg/mL, by the structure factor.

C. DLS on solutions crowded with SCNPs

Given the evidences for the presence of aggregates in the solutions with high SCNPs concentrations, a systematic investigation was performed by DLS to determine under which conditions the SCNPs aggregate and whether the complexes formed are again soluble upon dilution. This study was carried out on solutions of MNPs of M_w=124 kg/mol ($c^\star_{SCNP}$=68 mg/mL) and CuNPs of M_w=272 kg/mol ($c^\star_{SCNP}$=37 mg/mL). The experiments realized and their outcome, shown in the Supplemental Material, can be summarized as follows:

First, solutions of different concentrations (5, 10, 20 and 30 mg/mL) were prepared. DLS revealed unimolecular features for $c \leq$20 mg/mL and contributions from large objects for 30 mg/mL for the MNPs; in the case of CuNPs, isolated macromolecules were found for $c \leq$10 mg/mL, while aggregates were present already for 20 mg/mL. Thus, SCNPs seem to aggregate for concentrations above $c^\star_{SCNP}/3$ approximately.

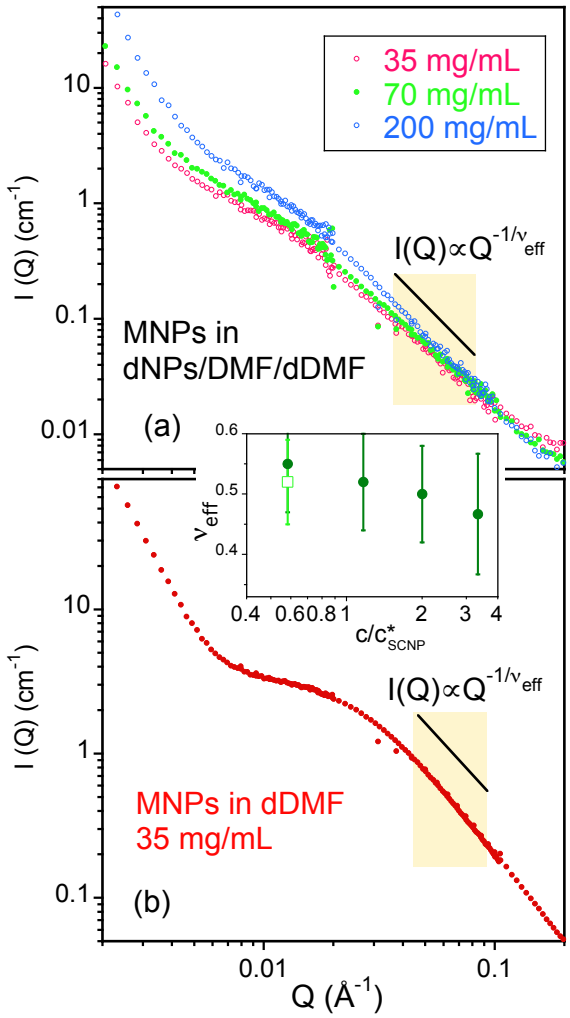

FIG. 7: SANS results on solutions of hydrogenated and deuterated Michael SCNPs in mixtures of dDMF/DMF for different polymer concentrations (see the text) (a) and on a solution of hydrogenated Michael SCNPs in dDMF at 35 mg/mL (b). The inset shows the concentration dependence of the scaling exponent obtained from the slopes in the fractal regime (indicated by the shadowed areas) from the solutions in (a) (solid circles) and in (b) (empty squares).

In order to check whether the aggregates are soluble again, we started from solutions at 200 mg/mL. These were progressively diluted again, up to 5 mg/mL in different steps. We found that CuNPs-solutions form gel-like structures in the concentration range 200$\geq$ c $\geq$50 mg/mL; at lower concentrations (c $\sim$30 mg/mL) the system behaves as a viscous liquid and becomes liquid-like for c $\leq$30 mg/mL. However, only after several ($\sim$8) days uni-molecular entities are obtained. Recovering solutions of isolated macromolecules turns to be impossible for MNPs-systems. In this case, the aggregates cannot be dissolved, even under high dilution conditions (5 mg/mL) and waiting for very long times.

We also diluted the starting 200 mg/mL-solutions to 5 mg/mL in one single shot. The systems with CuNPs recovered the uni-molecular character after one week; however, for MNPs solutions waiting did not help: even after two weeks the aggregates persisted.

We note that similar experiments carried out on low-M_w MNPs solutions gave the same results as those obtained for the M_w=124 kg/mol SCNPs above described.

D. MD-simulations

Now we test the former experimental results in the generic bead-spring model, which captures the universal monomer excluded volume and chain connectivity, and by construction is free of specific interactions and of both intra- and inter-molecular reactions in the solutions. Fig. 8 shows the form factor for the SCNPs in the solutions with linear crowders LIN50. Data are shown for concentrations from high dilution to the highest investigated one (about seven times the overlap concentration $c^*_{\rm SCNP}$ of the SCNPs). The form factor is calculated directly from the simulation coordinates as

$$P(Q) = \left\langle \frac{1}{N} \sum_{j,k} \exp\left[i\mathbf{Q}\cdot(\mathbf{r}_j - \mathbf{r}_k)\right] \right\rangle \ , \tag{9}$$

where the sum is restricted over monomers belonging to the same SCNP. We find in Fig. 8, as well as in the SCNP form factors for the other solutions (not shown), analogous trends to the experimental results of Fig. 3. Thus, increasing the concentration of crowders leads to a progressive reduction of the SCNP size and compaction of their conformations (decreasing $\overline{R}_{\rm g}$ and exponent ν in the fractal regime $P(Q) \sim Q^{-1/\nu}$).

Fig. 9 shows the simulation results for the average radius of gyration and the scaling exponent of the SCNPs, as a function of the total monomer concentration of the solu-

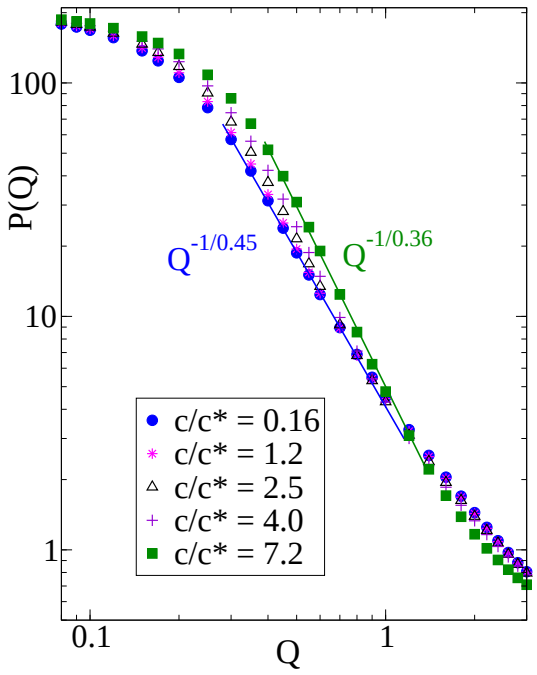

FIG. 8: Form factors of the SCNPs in the solutions with LIN50 crowders at different concentrations. Lines indicate power-law behavior $P(Q) \sim Q^{-1/\nu}$.

tion. Whereas the ν-exponents are again obtained by analyzing $P(Q)$, the calculation of $\overline{R}_{\rm g} = \langle R_{\rm g}^2 \rangle^{1/2}$ is more accurate than in the experiments since it is directly computed from the simulation data. The different data sets in Fig. 9 correspond to the different used crowders (the SCNPs in the pure systems and the linear chains LIN10, LIN50, LIN800 in the mixtures). We find the same trends as in the experiments. The analysis reveals unambiguously that in all cases the collapse of the SCNPs starts at their overlap concentration irrespective of the nature of the crowders. Indeed the overlap concentrations of the linear crowders with $N = 10$ and 800 are much higher and lower, respectively, than the corresponding value for the SCNPs (see vertical lines in Fig. 9). The confirmation of the experimental results in a generic bead-spring model suggests that the former finding is a universal feature of SCNPs in macromolecular solutions.

Close inspection of the different data sets reveals a non-trivial dependence of the SCNP collapse on the length N of the linear crowders. For a fixed concentration $c \gg c^*_{\rm SCNP}$ the SCNPs exhibit a stronger collapse by increasing N from 10 to 50. For $N = 50$ the SCNPs approach the maximum collapse observed in the investigated solutions, which corresponds to the case of using the SCNPs themselves as crowders. It is worth noting that the radius

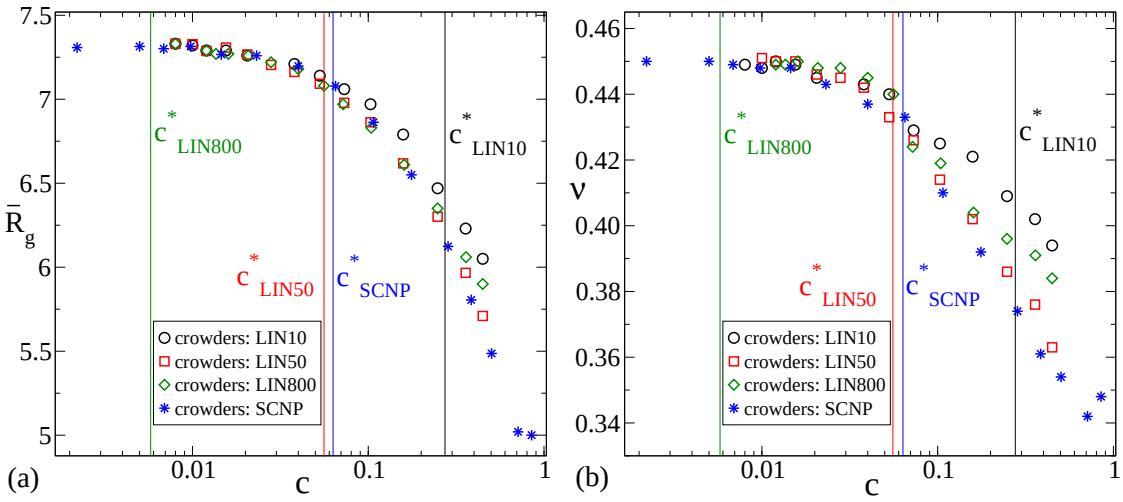

FIG. 9: Average radius of gyration (a) and scaling exponent (b) of the simulated SCNPs when linear precursor chains and SCNPs are used as crowding elements, as a function of the monomeric concentration. The vertical lines indicate the overlap concentrations of the SCNPs and the different linear crowders.

of gyration of the crowders increases by following the sequence LIN10 → LIN50 → SCNP (see Table III). A stronger SCNP collapse by increasing the crowder size is also apparently found in the experiments, as reflected by the red diamonds in Fig 6b corresponding to the same (Me-MNP) nanoparticles in solution with Lo-dPMMA (full symbols) and Me-dPMMA (empty symbols) crowders. It is also worth noting that the former experimental and MD-systems cover a qualitatively similar range of SCNP and crowder sizes (see the corresponding data in Tables I and III). Similar findings have been observed in the experiments by fixing the size of the linear crowder (Lo-dPMMA) and changing the size of the SCNP (Lo-, Me- and Hi-MNP), see Fig. 6). All the former results reflect the apparent fact that decreasing the size ratio SCNP/crowder leads to a stronger SCNP collapse . However, this is not always the case, and the trend is indeed reversed in the simulations by further increasing the length of the linear precursors to $N = 800$. In the presence of LIN800-crowders the SCNPs still show a stronger compaction than by using LIN10-crowders, but the compaction is weaker than that induced by the LIN50- and SCNP-crowders. It seems that the reentrance in the steepness of the collapse behavior occurs when the crowders become much larger than the SCNPs (the LIN800-crowders are about three times bigger than the SCNPs, see Table III). Unfortunately there was no counterpart with this size ratio in the real solutions and the

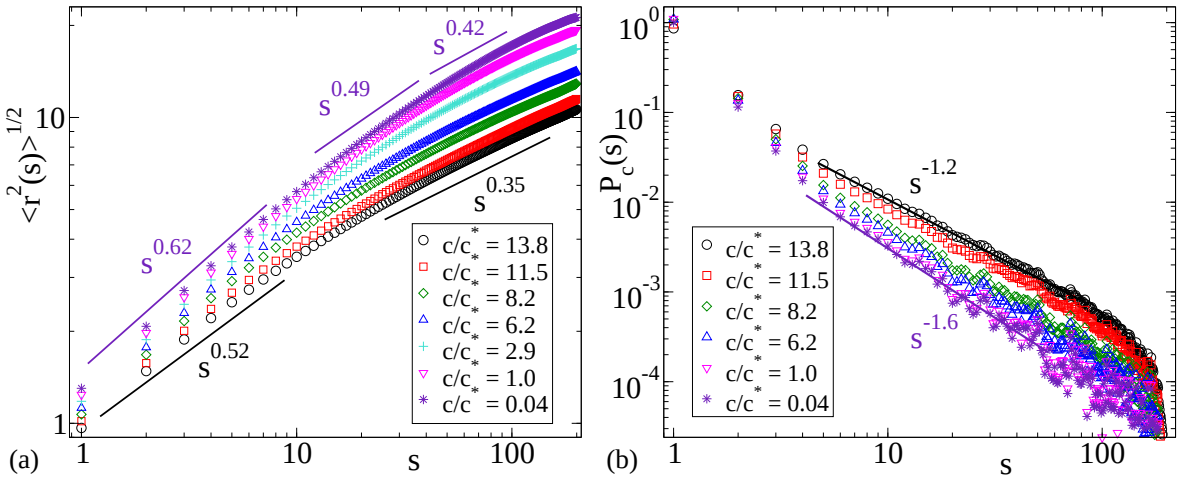

FIG. 10: (a): Average real distance vs contour distance. (b): Contact probability distribution. Symbols are MD-data for pure solutions of SCNPs at different concentrations. Data for $c/c^* = 13.8$ qualitatively correspond to the bulk state. For the sake of clarity, the data sets have been shifted vertically by factors 1.05^n (a) and 1.05^{-n} (b), with $n = 1, 2, 3, ...$ by going from the highest to the lowest concentration. Lines indicate approximate power-law behaviour.

reentrance could not be tested experimentally by now. This shall be the focus of future work.

Once checked that the simulations follow in general the same trends as the experimental results, further insight on the effect of crowding on the conformations of the SCNPs can be obtained by analysizing observables that cannot be directly accessed by the SANS experiments. Examples of such observables are given in Fig. 10. All data sets in both panels correspond to the pure SCNP solutions, where the whole concentration range, from high dilution to bulk density, has been studied. Fig. 10a shows the average real-space distance $\langle r^2(s)\rangle^{1/2}$ between two monomers in the SCNP separated by a contour distance s. By labelling the monomers as $i = 1, 2, ...N$ from one end to the other one in the backbone of the corresponding precursor, the contour distance between monomers i, j is just defined as $s = |i - j|$. Fig. 10b shows the contact probability distribution $P_c(s)$ between two monomers in the SCNP separated by a contour distance s. We consider that two monomers i, j are in contact if their real-space mutual distance is $r_{ij} < r_0 = r_c = 2^{1/6}\sigma$.

For comparison, in Fig. 10a we include lines representing power-law behavior $\langle r^2(s)\rangle^{1/2} \sim s^\nu$. Though the SCNPs are not large enough to exhibit well-defined, broad power-law

regimes, several trends in the real-space distance can be appreciated by increasing the contour distance and the concentration of the solution. For high dilution ($c/c^* \ll 1$) and small countour distances ($s < 10$) an effective exponent $\nu \approx 0.6$ is found. This behavior is close to that ideally expected for self-avoiding chains ($\langle r^2(s)\rangle^{1/2} \sim s^{\nu_F} = s^{0.59}$). At longer distances an exponent $0.4 < \nu < 0.5$ is found in consistency with the exponents found for the form factors at high dilution (Fig. 9b), and resembling the behavior expected for Gaussian chains in θ-solvent ($\nu = 1/2$). As aforementioned, the self-avoiding conformations of the precursor chains strongly favour bonding over short contour distances. This mechanism is inefficient for global compaction and just promotes the formation of very small local globules in the SCNP, in analogy with the structures adopted by chains and rings in θ-solvent. Though the total number of long loops per SCNP is too low to generate a compact topology, a significant fraction of SCNPs have some loop of length $N/2 < l < N$ monomers [49]. By moving along the contour of a loop the real-space distance stops growing beyond some point when the trajectory goes back to the origin. Thus, the partial contribution of the SCNPs having some long loop rationalizes the flattening of $\langle r^2(s)\rangle^{1/2}$ at $s > 100$ observed at high dilution.

By increasing the concentration of the solution beyond the overlap concentration the effective exponents in $\langle r^2(s)\rangle^{1/2}$ decrease. In concentrated solutions and in the bulk (black symbols in Fig. 10) an exponent $\nu \approx 0.5$ is found for $s < 10$, indicating that at small scales the SCNP strands are similar to Gaussian chains. However their large-scale arrangement is rather different. Data at long s can be described by an effective exponent $\nu \sim 0.35$, in consistency with the exponents found in the form factors for $c \gg c^*$ (Fig. 9b). As anticipated by the analysis of the form factors, the observation of an exponent $\nu \sim 1/3$ in the scaling behaviour of $\langle r^2(s)\rangle^{1/2}$ suggests analogies between the conformations of SCNPs in highly crowded environments and those of crumpled globular objects ($\nu = 1/3$). It must be noted that these are very different from the 'equilibrium' globular structures adopted by, e.g., collapsed linear chains in bad solvent. In that case $\langle r^2(s)\rangle^{1/2}$ would obey Gaussian statistics as linear chains in a melt ($\sim s^{1/2}$), and an ultimate plateau would emerge at $s \approx (3N/4\pi)^{2/3} \approx 13$ where the radius of the confining sphere would be reached and the Gaussian paths would be bounced back [50, 51]. Morever, as aforementioned, equilibrium globular conformations would be reflected by Porod scattering in the form factor, $P(Q) \sim Q^{-4}$, which has not been the case.

An important test of the analogy between the SCNP conformations in crowded solutions

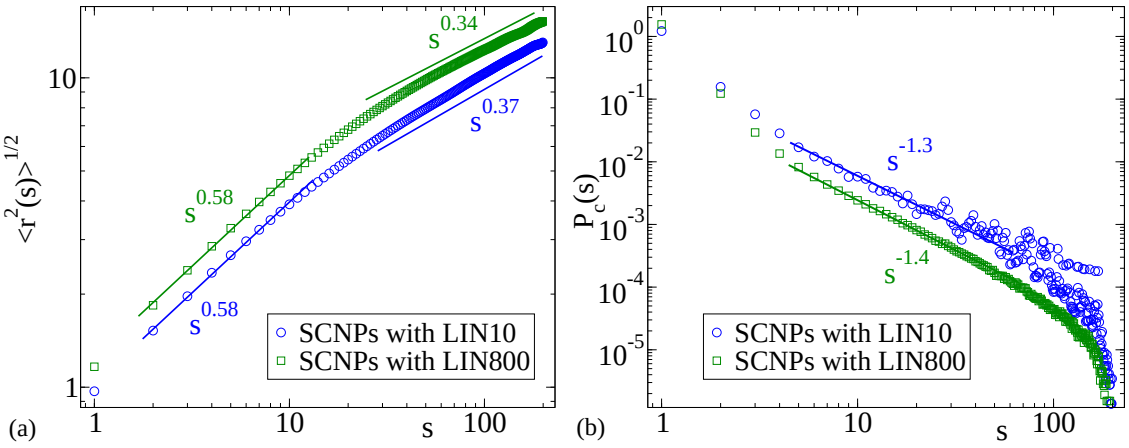

FIG. 11: Average real distance vs contour distance (a), and contact probability distribution (b) for SCNPs in solution with LIN10 and LIN800 crowders at total monomer concentration $c = 7.2c^*_{\rm SCNP}$. For the sake of clarity, the upper set in (a) (green symbols) has been shifted vertically by a factor 1.2. Lines indicate approximate power-law behaviour.

and those of crumpled globules can be obtained by observing the scaling behavior of the contact probability distribution. As shown in Fig. 10b, the latter can be described by a power-law $P_{\rm c}(s) \sim s^{-x}$. At high dilution an exponent $x \approx 1.6$ is found for $5 < s < 100$, i.e., roughly in the same range of the approximate Gaussian behavior found in $\langle r^2(s)\rangle^{1/2}$ (Fig. 10a). The exponent $x \approx 1.6$ can indeed be rationalized by invoking statistics of Gaussian linear chains, for which the return probability of a long segment ($s \gg 1$) [52] scales as $s^{-3/2}$. By crossing the overlap concentration the effective exponent decreases down to $x \approx 1.2$ at the bulk density. To the best of our knowledge, no rigorous calculation has been reported in the literature for the exponent x characteristic of the crumpled globule. Still an estimation (it is strictly inexact, see discussion in Ref. [40]) by using mean-field arguments yields $x = 3\nu = 1$ [40]. The observation $x \gtrsim 1$, as previously found for melts of ring polymers and chromatin loops in chromosomes [40, 42, 51, 53], confirms the structural analogies between the conformations of SCNPs in crowded solutions and those of crumpled globular objects. It is worth stressing that the former results for the x-exponents are not sensitive to any reasonable choice $0.9 \leq r_0/r_{\rm c} \leq 1.1$ for the contact criterion $r < r_0$.

Similar findings to those of Fig. 10 are observed in the mixtures. Fig. 11 shows results of $\langle r^2(s)\rangle^{1/2}$ and $P_{\rm c}(s)$ for the SCNPs in the mixtures with the LIN10 and LIN800 crowders, at the highest investigated concentration $c = 7.2c^*_{\rm SCNP}$. This corresponds to a monomer

concentration $c = 0.49$, still far from the bulk-like value $c = 0.85$. This is the reason why the scaling of $\langle r^2(s)\rangle^{1/2}$ at local scales ($s < 10$) still reflects self-avoiding behavior ($\nu \lesssim \nu_{\mathrm{F}} = 0.59$) instead of Gaussian-like ($\nu = 0.5$). However, crowding induces apparent compaction into crumpled globular conformations, as suggested by the exponents $\nu \approx 0.37$ and 0.34 obtained at long contour distances. The contact probability distribution shows scaling behavior $P(s) \sim s^{-x}$, where the observed exponents $x = 1.3$ and 1.4 are higher than that found in the pure melt of SCNPs ($x = 1.2$) and far from the ideal mean-field prediction $x = 1$. In general, the observations in Fig. 11 are consistent with the weaker compaction of the SCNPs in the mixtures than in the pure SCNP solution at the same monomer concentration (as shown in Fig. 9). The results of $\langle r^2(s)\rangle^{1/2}$ and $P_{\mathrm{c}}(s)$ for the SCNPs in the mixtures with LIN50 crowders (not shown) are closer to those found in the pure SCNP, again in consistency with the results in Fig. 9. Anyway, in all systems clear indications are found, through the scaling exponents of the different computed observables, for the development of the crumpled globular structures of the SCNPs already at concentrations of about half the bulk density.

V. DISCUSSION

A. Reversibility of aggregation

SANS and DLS experiments have demonstrated the formation of supramolecular aggregates for concentrated solutions of SCNPs, namely for concentrations above approx. $c^{\star}_{SCNP}/3$. This aggregation phenomenon is absent in the solutions crowded with linear PMMA chains, where the concentrations of SCNPs remains low. Thus, SCNPs tend to react with similar entities above a concentration threshold. The mechanism presumably consists of inter-molecular reactions mediated by functionalized AEMA groups of different SCNPs that do not participate in the intra-molecular cross-link network generated during the SCNPs synthesis. In concentrated conditions, the probability of close spatial proximity between such unreacted groups increases and interactions might occur. We note that the creation of a single inter-molecular bond leads already to the fomation of a dimer.

The reversibility of the aggregation process is determined by the kind of reaction involved in the cross-linking synthesis route. Cu-complexation is a reversible mechanism leading thus

to aggregates of transitory character. On the contrary, the covalent nature of the cross-links induced in the synthesis by Michael addition obviously leads to permanent bonds between the functionalized groups of different macromolecules and consequently to irreversibility of the aggregation process.

For our experimental investigation on the role of crowding on the morphology of SCNPs, this aggregation phenomenon has posed strong difficulties, preventing reliable conclusions to be extracted from the SANS experiments. We note for example that the effective values of the scaling exponent deduced from the slope of the SANS curves in the intermediate Q-range –denoted as ν_{eff}– are much higher than those obtained from the crowding with linear (and inert) dPMMA crowders. Though they present the same tendency to drecrease with increasing concentration above $c^{\star}_{SCNP}$, they cannot be considered as trustworthy.

B. Crossover at c^{*}_{SCNP} and collapse behavior

The main result from our joint study involving experiments and MD-simulations is the univocal determination of the overlap concentration of the SCNPs as the key magnitude determining the onset of the crossover from unperturbed morphology at lower concentrations to an increasingly collapsed state at higher concentrations. This has been demonstrated by experiments on solutions with SCNPs of different sizes crowded with linear macromolecules of both, smaller and larger dimensions than the SCNPs. These results have been nicely corroborated by extensive MD-simulations on mixtures of SCNPs and linear chains, covering a large range of relative sizes. In addition, free from unwanted inter-molecular cross-linking reactions, MD-simulations have extended this investigation to the case where the environment of the SCNPs is crowded also with similar entities.

An interesting observation from the simulations is that increasing the size of the linear crowders at fixed high monomer concentration initially leads to a stronger collapse of the SCNPs, but when the crowders become too large (several times the SCNP size, as in the LIN800 case) this trend is reversed. Exploring the case of longer crowders ($N \gg 800$) would be computationally very involved because of the need of much longer boxes and equilibration times (scaling as N^3 since they are already in the entangled regime [47]). Still, increasing the size of the linear crowder beyond some limit should not further influence the collapse behavior of the SCNP, since a segment of the same size as the SCNP will be just a small

fraction of the linear chain and its typical spatial arrangement within the cloud of SCNP monomers will not be further modified.

The microscopic mechanism for the non-monotonicity of the SCNP collapse behavior is not clear. Some insight might be expected by identifying surface contacts per SCNP, these being defined as the average number of contacts, $n_{\rm surf}$, between monomers in the SCNP and in another macromolecule (again using $r < r_{\rm c} = 2^{1/6}\sigma$ as the contact criterion). At the highest common concentration that has been investigated, $c = 7.2c^*_{\rm SCNP}$, we find the values $n_{\rm surf} \approx 40, 34, 26$ and 10 for the SCNPs in the solutions with the crowders LIN10, LIN50, SCNP and LIN800, respectively.

Since following the crowder sequence LIN10 $\rightarrow$ LIN50 $\rightarrow$ SCNP leads to a stronger collapse of the SCNP at fixed concentration (Fig. 9), it becomes clear that stronger collapse is actually not related to the mean-field picture based on the number of surface contacts between SCNPs and crowders, but to the spatial arrangement of the crowder monomers within the cloud of the SCNP. By increasing the crowder size (as it happens in the sequence LIN10 $\rightarrow$ LIN50 $\rightarrow$ SCNP, see Table III) the number of such possible arrangements decreases due to connectivity constraints, leading to the depletion of the SCNPs, which need to form more compact configurations, from the uncrossable long segments of the crowders. When the latter become much longer than the SCNP size (as in the case of the LIN800 crowders) there is a relative swelling of the SCNPs with respect to the solutions with shorter crowders. A temptative explanation for such a relative swelling might be that when linear crowders are too long the only way to pervade the volume occupied by the SCNP is through some threading events.

As aforementioned, crumpled globular behavior has been previously observed in melts of ring polymers [40]. In this work we have shown that the crumpled globular conformations of the SCNPs are not only found in the concentrated pure solutions (MD-results), but also when the SCNPs are very diluted in the crowded solutions of linear chains (experiments and MD), i.e., even when SCNP-SCNP contacts are negligible and each SCNP is basically surrounded by linear chains. This is *not* the case for ring polymers, which adopt Gaussian-like conformations when they are diluted in a melt of linear chains [54, 55]. In connection with the discussion in the former paragraph, the presence, unlike in rings, of mutually *cross-linked* loops in the SCNPs [20] makes them relatively unthreadable [56], and facilitates a stronger collapse than rings to accomodate the presence of the linear crowders in their

surroundings.

VI. SUMMARY AND CONCLUSIONS

We have presented an investigation, by combining small-angle neutron scattering (SANS) and molecular dynamics (MD) simulations, on the conformational properties of single-chain nano-particles (SCNPs) in crowded macromolecular solutions. Crowding was induced by two means, namely by adding either linear polymer chains or SCNPs. The main conclusions can be summarized as follows:

- By using linear chains as crowders we find a crossover from almost unperturbed SCNP conformations in dilute conditions toward a continuous collapse of the macromolecule with increasing crowding. Using two very different molecular weights of the linear crowders we show that the overlap concentration of the SCNP is the key factor determining the crossover toward compaction. SCNPs start to collapse when the total concentration of the solution (diluted SCNPs and increasing crowders) reaches the value of the overlap concentration of the pure SCNP solutions, irrespective of the length of the crowders.

- The experiments inducing crowding by increasing the SCNPs concentration (as previously investigated by MD-simulations [20]) turned out to be more complicated, revealing the presence of aggregates. By means of DLS we have shown that unavoidable aggregation occurs when the concentration of SCNPs reaches approximately one third of their overlap concentration $c^\star$. For high concentrations, even a gel-like structure is observed. Unimolecular solutions are recovered upon dilution only for solutions of SCNPs obtained by reversible crosslinking. Despite aggregation, some information about chain compaction could be extracted from the SANS results that indicates the same behavior of SCNPs as observed in the solutions with linear chains, regarding the coincidence of the onset of collapse with the overlap concentration of the SCNPs.

- The generalizability of these experimental findings is supported by MD-simulations using a generic 'bead-spring' coarse-grained model. The simulations, which have used both SCNPs and linear crowders with overlap concentrations *much lower and much higher* than that of the SCNPs, unambiguously confirm that the onset of the SCNP

collapse occurs at the total monomer concentration corresponding to the overlap concentration of the SCNPs. Moreover, the analysis of the scaling behavior of the different simulation observables confirms the trends suggested by the experimental form factors, and suggests that crumpled globular conformations are generally adopted by SCNPs in crowded macromolecular solutions. In the case of linear crowders, the SCNPs show, at fixed monomer concentration, a non-monotonic dependence of their collapse on the length of the crowders.

VII. ACKNOWLEDGEMENTS

We thank I. Asenjo and A. Iturrospe for help with the sample synthesis and assistance during the experiments. We acknowledge financial support by the Spanish Ministry 'Ministerio de Economia y Competitividad', code: MAT2015-63704-P (MINECO/FEDER, UE) and by the Basque Government IT-654-13 (GV). This work is based on experiments performed at JCNS-instrument KWS-2 (Heinz Maier-Leibnitz Zentrum (MLZ), Garching, Germany) and has been supported by the European Commission under the 7th Framework Programme through the 'Research Infrastructures' action of the 'Capacities' Programme, NMI3-II Grant Number 283883.

---

[1] Perez-Baena, I.; Barroso-Bujans, F.; Gasser, U.; Arbe, A.; Moreno, A. J.; Colmenero, J.; Pomposo, J. A. Endowing Single-Chain Polymer Nanoparticles with Enzyme-Mimetic Activity. *ACS Macro Letters* **2013**, *2*, 775–779.

[2] Sanchez-Sanchez, A.; Arbe, A.; Colmenero, J.; Pomposo, J. A. Metallo-Folded Single-Chain Nanoparticles with Catalytic Selectivity. *ACS Macro Letters* **2014**, *3*, 439–443.

[3] Huerta, E.; Stals, P. J. M.; Meijer, E. W.; Palmans, A. R. A. Consequences of Folding a Water-Soluble Polymer Around an Organocatalyst. *Angewandte Chemie International Edition* **2013**, *52*, 2906–2910.

[4] Terashima, T.; Mes, T.; De Greef, T. F. A.; Gillissen, M. A. J.; Besenius, P.; Palmans, A. R. A.; Meijer, E. W. Single-Chain Folding of Polymers for Catalytic Systems in Water. *Journal of the American Chemical Society* **2011**, *133*, 4742–4745.

[5] Altintas, O.; Barner-Kowollik, C. Single-Chain Folding of Synthetic Polymers: A Critical Update. *Macromol. Rapid Commun.* **2016**, *37*, 29–46.

[6] Lyon, C. K.; Prasher, A.; Hanlon, A. M.; Tuten, B. T.; Tooley, C. A.; Frank, P. G.; Berda, E. B. A brief user's guide to single-chain nanoparticles. *Polym. Chem.* **2015**, *6*, 181–197.

[7] Gonzalez-Burgos, M.; Latorre-Sanchez, A.; Pomposo, J. A. Advances in single chain technology. *Chem. Soc. Rev.* **2015**, *44*, 6122–6142.

[8] Mavila, S.; Eivgi, O.; Berkovich, I.; Lemcoff, N. G. Intramolecular Cross-Linking Methodologies for the Synthesis of Polymer Nanoparticles. *Chem. Rev.* **2016**, *116*, 878–961.

[9] Hanlon, A. M.; Lyon, C. K.; Berda, E. B. What Is Next in Single-Chain Nanoparticles? *Macromolecules* **2016**, *49*, 2–14.

[10] Pomposo, J. A., Ed. *Single-Chain Polymer Nanoparticles: Synthesis, Characterization, Simulations, and Applications*; John Wiley & Sons: Weinheim, Germany, 2017.

[11] Pomposo, J. A.; Perez-Baena, I.; Lo Verso, F.; Moreno, A. J.; Arbe, A.; Colmenero, J. How Far Are Single-Chain Polymer Nanoparticles in Solution from the Globular State? *ACS Macro Letters* **2014**, *3*, 767–772.

[12] Moreno, A. J.; Lo Verso, F.; Sanchez-Sanchez, A.; Arbe, A.; Colmenero, J.; Pomposo, J. A. Advantages of Orthogonal Folding of Single Polymer Chains to Soft Nanoparticles. *Macromolecules* **2013**, *46*, 9748–9759.

[13] Stadler, A. M.; Stingaciu, L.; Radulescu, A.; Holderer, O.; Monkenbusch, M.; Biehl, R.; Richter, D. Internal Nanosecond Dynamics in the Intrinsically Disordered Myelin Basic Protein. *Journal of the American Chemical Society* **2014**, *136*, 6987–6994, PMID: 24758710.

[14] Habchi, J.; Tompa, P.; Longhi, S.; Uversky, V. N. Introducing Protein Intrinsic Disorder. *Chem. Rev.* **2014**, *114*, 6561–6588.

[15] Marsh, J. A.; Forman-Kay, J. D. Sequence Determinants of Compaction in Intrinsically Disordered Proteins. *Biophys. J.* **2010**, *98*, 2383–2390.

[16] Hofmann, H.; Soranno, A.; Borgia, A.; Gast, K.; Nettels, D.; Schuler, B. Polymer scaling laws of unfolded and intrinsically disordered proteins quantified with single-molecule spectroscopy. *Proc. Natl. Acad. Sci.* **2012**, *109*, 16155–16160.

[17] Lo Verso, F.; Pomposo, J. A.; Colmenero, J.; Moreno, A. J. Simulation guided design of globular single-chain nanoparticles by tuning the solvent quality. *Soft Matter* **2015**, *11*, 1369–1375.

[18] Lo Verso, F.; Pomposo, J. A.; Colmenero, J.; Moreno, A. J. Multi-orthogonal folding of single polymer chains into soft nanoparticles. *Soft Matter* **2014**, *10*, 4813–4821.

[19] Rabbel, H.; Breier, P.; Sommer, J.-U. Swelling Behavior of Single-Chain Polymer Nanoparticles: Theory and Simulation. *Macromolecules* **2017**, *50*, 7410–7418.

[20] Moreno, A. J.; Lo Verso, F.; Arbe, A.; Pomposo, J. A.; Colmenero, J. Concentrated Solutions of Single-Chain Nanoparticles: A Simple Model for Intrinsically Disordered Proteins under Crowding Conditions. *The Journal of Physical Chemistry Letters* **2016**, *7*, 838–844, PMID: 26894933.

[21] Arbe, A.; Pomposo, J.; Moreno, A.; LoVerso, F.; Gonzlez-Burgos, M.; Asenjo-Sanz, I.; Iturrospe, A.; Radulescu, A.; Ivanova, O.; Colmenero, J. Structure and dynamics of single-chain nano-particles in solution. *Polymer* **2016**, *105*, 532–544, Structure and Dynamics of Polymers studied by X-ray, Neutron and Muon Scattering.

[22] Ellis, R. Macromolecular crowding: an important but neglected aspect of the intracellular environment. *Current Opinion in Structural Biology* **2001**, *11*, 114–119.

[23] Ellis, R. J.; Minton, A. P. Cell biology: Join the crowd. *Nature* **2003**, *425*, 27–28.

[24] Zhou, H.-X.; Rivas, G.; Minton, A. P. Macromolecular Crowding and Confinement: Biochemical, Biophysical, and Potential Physiological Consequences. *Annual Review of Biophysics* **2008**, *38*, 375–397.

[25] McGuffee, S. R.; Elcock, A. H. Diffusion, Crowding & Protein Stability in a Dynamic Molecular Model of the Bacterial Cytoplasm. *PLoS Computational Biology* **2010**, *6*, e1000694.

[26] Elcock, A. H. Models of macromolecular crowding effects and the need for quantitative comparisons with experiment. *Current Opinion in Structural Biology* **2010**, *20*, 196–206, Theory and simulation / Macromolecular assemblages.

[27] Kuznetsova, I. M.; Turoverov, K. K.; Uversky, V. N. What Macromolecular Crowding Can Do to a Protein. *International Journal of Molecular Sciences* **2014**, *15*, 23090–23140.

[28] Latshaw, D. C.; Cheon, M.; Hall, C. K. Effects of Macromolecular Crowding on Amyloid Beta (1622) Aggregation Using Coarse-Grained Simulations. *The Journal of Physical Chemistry B* **2014**, *118*, 13513–13526.

[29] Zhou, H.-X. Influence of crowded cellular environments on protein folding, binding, and oligomerization: Biological consequences and potentials of atomistic modeling. *FEBS Letters* **2013**, *587*, 1053–1061.

[30] Stagg, L.; Zhang, S.-Q.; Cheung, M. S.; Wittung-Stafshede, P. Molecular crowding enhances native structure and stability of / protein flavodoxin. *Proceedings of the National Academy of Sciences* **2007**, *104*, 18976–18981.

[31] Cheung, M. S.; Klimov, D.; Thirumalai, D. Molecular crowding enhances native state stability and refolding rates of globular proteins. *Proceedings of the National Academy of Sciences of the United States of America* **2005**, *102*, 4753–4758.

[32] Kim, Y. C.; Bhattacharya, A.; Mittal, J. Macromolecular Crowding Effects on Coupled Folding and Binding. *The Journal of Physical Chemistry B* **2014**, *118*, 12621–12629.

[33] Theillet, F.-X.; Binolfi, A.; Frembgen-Kesner, T.; Hingorani, K.; Sarkar, M.; Kyne, C.; Li, C.; Crowley, P. B.; Gierasch, L.; Pielak, G. J.; Elcock, A. H.; Gershenson, A.; Selenko, P. Physicochemical Properties of Cells and Their Effects on Intrinsically Disordered Proteins (IDPs). *Chemical Reviews* **2014**, *114*, 6661–6714.

[34] Johansen, D.; Jeffries, C. M.; Hammouda, B.; Trewhella, J.; Goldenberg, D. P. Effects of Macromolecular Crowding on an Intrinsically Disordered Protein Characterized by Small-Angle Neutron Scattering with Contrast Matching. *Biophysical Journal* **2011**, *100*, 1120–1128.

[35] Qin, S.; Zhou, H.-X. Effects of Macromolecular Crowding on the Conformational Ensembles of Disordered Proteins. *The Journal of Physical Chemistry Letters* **2013**, *4*, 3429–3434.

[36] Cino, E. A.; Karttunen, M.; Choy, W.-Y. Effects of Molecular Crowding on the Dynamics of Intrinsically Disordered Proteins. *PLOS ONE* **2012**, *7*, e49876.

[37] Mackay, M. E.; Dao, T. T.; Tuteja, A.; Ho, D. L.; van Horn, B.; Kim, H.-C.; Hawker, C. J. Nanoscale effects leading to non-Einstein-like decrease in viscosity. *Nature Materials* **2003**, *2*, 762–766.

[38] Arbe, A.; Pomposo, J. A.; Asenjo-Sanz, I.; Bhowmik, D.; Ivanova, O.; Kohlbrecher, J.; Colmenero, J. Single Chain Dynamic Structure Factor of Linear Polymers in an All-Polymer Nano-Composite. *Macromolecules* **2016**, *49*, 2354–2364.

[39] Grosberg, A. Yu.,; Nechaev, S.K.,; Shakhnovich, E.I., The role of topological constraints in the kinetics of collapse of macromolecules. *J. Phys. France* **1988**, *49*, 2095–2100.

[40] Halverson, J. D.; Lee, W. B.; Grest, G. S.; Grosberg, A. Y.; Kremer, K. Molecular dynamics simulation study of nonconcatenated ring polymers in a melt. I. Statics. *The Journal of Chemical Physics* **2011**, *134*, 204904.

[41] Gooßen, S.; Brás, A. R.; Krutyeva, M.; Sharp, M.; Falus, P.; Feoktystov, A.; Gasser, U.; Pyckhout-Hintzen, W.; Wischnewski, A.; Richter, D. Molecular Scale Dynamics of Large Ring Polymers. *Phys. Rev. Lett.* **2014**, *113*, 168302.

[42] Halverson, J. D.; Smrek, J.; Kremer, K.; Grosberg, A. Y. From a melt of rings to chromosome territories: the role of topological constraints in genome folding. *Reports on Progress in Physics* **2014**, *77*, 022601.

[43] Sanchez-Sanchez, A.; Akbari, S.; Etxeberria, A.; Arbe, A.; Gasser, U.; Moreno, A. J.; Colmenero, J.; Pomposo, J. A. Michael Nanocarriers Mimicking Transient-Binding Disordered Proteins. *ACS Macro Letters* **2013**, *2*, 491–495.

[44] Kremer, K.; Grest, G. S. Dynamics of entangled linear polymer melts: A molecular-dynamics simulation. *J. Chem. Phys.* **1990**, *92*, 5057–5086.

[45] Fetters, L. J.; Lohse, D. J.; Colby, R. H. *Physical Properties of Polymers Handbook*; Springer New York: New York, NY, 2007; pp 447–454.

[46] Hess, B.; Kutzner, C.; van der Spoel, D.; Lindahl, E. GROMACS 4: Algorithms for Highly Efficient, Load-Balanced, and Scalable Molecular Simulation. *J. Chem. Theory Comput.* **2008**, *4*, 435–447.

[47] Rubinstein, M.; Colby, R. H. *Polymer Physics*; Oxford: Oxford University Press, 2003.

[48] Hammouda, B. Small-Angle Scattering From Branched Polymers. *Macromolecular Theory and Simulations* **2012**, *21*, 372–381.

[49] A.J. Moreno, P. Bacova, F. Lo Verso, A. Arbe, J. Colmenero, and J.A. Pomposo, submitted.

[50] Grosberg, A. Y.; Nechaev, S. K.; Shakhnovich, E. I. The role of topological constraints in the kinetics of collapse of macromolecules. *J. Phys. (Paris)* **1988**, *49*, 2095–2100.

[51] Mirny, L. A. The fractal globule as a model of chromatin architecture in the cell. *Chromosome Res.* **2011**, *19*, 37–51.

[52] Lua, R.; Borovinskiy, A. L.; Grosberg, A. Y. Fractal and statistical properties of large compact polymers: a computational study. *Polymer* **2004**, *45*, 717–731.

[53] Rosa, A.; Becker, N. B.; Everaers, R. Looping Probabilities in Model Interphase Chromosomes. *Biophys. J.* **2010**, *98*, 2410–2419.

[54] Halverson, J. D.; Grest, G. S.; Grosberg, A. Y.; Kremer, K. Rheology of Ring Polymer Melts: From Linear Contaminants to Ring-Linear Blends. *Phys. Rev. Lett.* **2012**, *108*, 038301.

[55] Gooßen, S.; Krutyeva, M.; Sharp, M.; Feoktystov, A.; Allgaier, J.; Pyckhout-Hintzen, W.;

Wischnewski, A.; Richter, D. Sensing Polymer Chain Dynamics through Ring Topology: A Neutron Spin Echo Study. *Phys. Rev. Lett.* **2015**, *115*, 148302.

[56] Bačová, P.; Lo Verso, F.; Arbe, A.; Colmenero, J.; Pomposo, J. A.; Moreno, A. J. The Role of the Topological Constraints in the Chain Dynamics in All-Polymer Nanocomposites. *Macromolecules* **2017**, *50*, 1719–1731.

FOR TABLE OF CONTENTS USE ONLY

'Crowding the Environment of Single-Chain Nano-Particles:

A Combined Study by SANS and Simulations'

Marina González-Burgos, Arantxa Arbe, Angel J. Moreno, José A. Pomposo, Aurel Radulescu and Juan Colmenero